Tapered side-polished microfibre sensor for high sensitivity hCG detection

Wei Luo, Bin Liu*, Juan Liu, Tao Wu, Qiang Liu, Meng-Yu Wang, Sheng-Peng Wan, Jinhui Yuan*, Ping Lu, Danling Wang, Xing-Dao He, and Qiang Wu*

***Abstract*—A high sensitivity human chorionic gonadotropin (hCG) detection was conducted by a tapered side-polished (TSP) optical fiber sensor. Experimentally, the TSP fiber sensor was made by side polishing a short section of single mode fiber to a D shape structure and tapering the D shape section to a small diameter (<10 μm in the experiments). By functionalizing the primary antibody of hCG onto the TSP fiber surface, the sensor was used for detecting hCG concentration. Experimental results show that when the hCG concentration is 0.1 mIU/mL, the sensor has an average wavelength shift of 0.82 nm. The limit of detection (LoD) of the hCG is estimated 0.058 mIU/mL, assuming three times of maximum wavelength variation (3×0.15=0.45 nm) in Phosphate buffer saline (PBS) to the measurement limit. The specificity has also been tested by immersing the sensor into a mixed biomaterial solution (hCG - 1 mIU/mL, pig-IgG - 1 μg/mL, Staphylococcus aureus - 6×10^5 CFU/mL and Escherichia coli - 2.5×10^5 CFU/mL). The result showed that the TSP optical fiber sensor has excellent specificity. The biosensor has potential application in clinical/medical diagnostics, human health, environmental quality and food safety monitoring.**

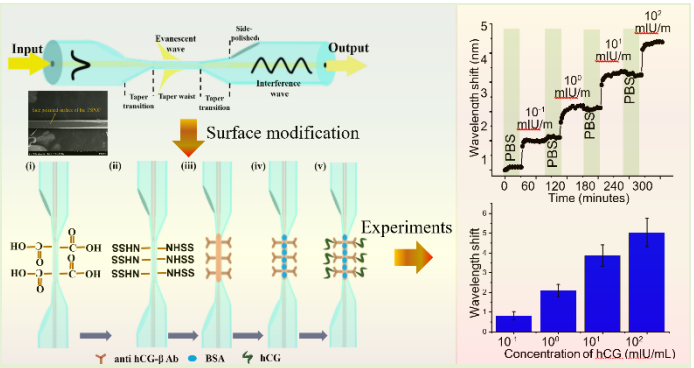

***Index Terms*— Optical microfiber, Biosensor, side-polished optical fiber, Refractive index, Human chorionic gonadotropin (hCG)**

I. Introduction

SINCE the first optical fiber sensor was reported in the late 1970s [1], optical fiber sensors have been developed by leaps and bounds. Benefiting from its outstanding properties like ultra-high sensitivity, robust to electromagnetic field and lightweight, optical fiber sensor has been widely used in different applications like physical, biomolecules, chemical and environment detection [2-4]. For example, the recent works of the optical fiber biosensors for Human chorionic gonadotropin [5], Escherchia coli bacteria [6] and Salmonella Typhimurium [7] detection. The common optical fiber sensor structures include Mach Zehnder interferometer (MZI), Multimode interferometer, Sagnac ring, Fabry-Perot cavity, fiber gratings[8]. Moreover, with the rapid development of micro/nano technology and the increasing demand for high-performance, multi-functional optical sensors, spatial miniaturization has become one of the current trends of optical

This work was jointly supported by the National Natural Science Foundation of China (NSFC) (62175097, 62065013, 11864025, 61865013); Nanchang Hangkong University graduate student innovation special fund project (YC2020-071); Natural Science Foundation of Jiangxi Province (20192ACB20031, 20192ACBL21051 and 20202ACBL202002), Key R&D Projects of the Ministry of Science and Technology of China (2018YFE0115700); Royal Society International Exchanges 2020 Cost Share (NSFC) (IEC\NSFC\201015) and National Natural Science Foundation of China-Royal Society Exchange Programme (62111530153). (Correspondence authors: Bin Liu, Qiang Wu and Jinhui Yuan)

Wei Luo, Bin Liu, , Juan Liu, Tao Wu, Meng-Yu Wang, Sheng-peng Wan, Xing-Dao He and Qiang Wu are with Key Laboratory of Opto-Electronic Information Science and Technology of Jiangxi Province, Nanchang Hangkong University, Nanchang, China (e-mail: liubin@nchu.edu.cn; qiang.wu@northumbria.ac.uk).

Qiang Wu is also with Faculty of Engineering and Environment, Northumbria University, Newcastle Upon Tyne NE1 8ST, UK.

Qiang Liu is with Hebei Key Laboratory of Micro-Nano Precision Optical Sensing and Measurement Technology, School of Control Engineering, Northeastern University at Qinhuangdao, Qinhuangdao, China

Jinhui Yuan is with the Research Center for Convergence Networks and Ubiquitous Services, University of Science & Technology Beijing, Beijing 100083, China. (e-mail: yuanjinhui81@163.com)

Ping Lu is with School of Optical and Electronic Information, Huazhong University of Science and Technology, Wuhan 430074, China

Danling Wang is with Department of Electrical and Computer Engineering, North Dakota State University, Fargo, ND 58102, USA.

fiber sensors [9]. Compared with the traditional optical fiber, the micro/nano optical fiber has a sub-wavelength structure, strong evanescent [10-13]. The micro/nano fiber optic sensor has advantages of rapid response, ultrahigh sensitivity, and excellent spatial resolution, and thus is becoming a new platform for sensing application. Typically, the microfiber structures include, microfiber coupler, microfiber interferometer, microfiber grating, microfiber resonators, etc. [14-18].

The tapered optical fiber (TOF) is one of the most common microfibers, which is attracting increasing research interest due to its advantages, like strong evanescent field and mode confinement, micro/nano-scale dimension and has been developed into a series of practical application value of devices. For example, the microfiber bottle resonator is normally formed by a section of TOF and a silica micro-bottle [19]; a combination of the fiber grating structure and fiber taper techniques to increase the sensing performance [20-22]; a microfiber knot resonator made by the TOF [23].

On the other hand, D-shaped optical fiber is attracting research interests due to its advantages of simple fabrication, strong mechanical stability and easy modification of sensing material on the surface due to the large and smooth side polished surface. Benefit from these advantages, D-shape optical fiber has been widely applied in sensing applications, including refractive index (RI), temperature, magnetic field and biochemical sensing [24]. However, the D-shape fiber suffers the disadvantage of relatively low sensitivity, limiting the application of D-shape fiber sensor, particularly in ultra-low concentration biochemical detections. In order to address this challenge, researchers proposed methods integrating various structures such as surface plasmonic resonant (SPR), whispering gallery modes (WGM), microstructures, and gratings into the D-shaped fiber, which demonstrated that the sensing performance has been improved significantly [25-32]. In addition, compared to hollow fiber and photonic optical fiber [25, 33], it is easier to flow analyte liquid through D-shaped fiber sensor.

Human chorionic gonadotropin (hCG) is a glycoprotein hormone consisting of two distinct subunits: α-hCG, which exists in different glycoprotein hormones [34], and β-hCG, which has a large glycosylated domain [35]. Compared with other glycoproteins, hCG is the product of trophoblasts and malignant tumors and is an indicator of pregnancy processes [36]. In pregnancy promoting process, the concentration of hCG is normally high and approximately >5 mIU/mL during the first pregnancy week. The clinical diagnostic method, such as the point-of-care (POC) testing method can be used to detect the hCG concentration. However, although the usual progesterone test stick is cheap, it cannot detect the low concentrations of hCG (<1 mIU/mL), which usually occurs in recurrent seminoma and a non-seminoma testicular tumor [37]. Therefore, as the diagnostic marker of pregnancy or early fatal loss, or as the tumor biomarker in organs such as pancreas, stomach and lung, the hCG detection is very important. In the past few years, several methods have been presented for hCG detection, such as fluorescent immunoassays, radioimmunoassay, enzyme linked immunosorbent assay (ELISA), electrochemiluminescence, SPR and so on. The optical microfiber sensor is an emerging technique for biosensing and attracted wide interests for hCG detection [5, 38, 39].

In this paper, a high sensitivity hCG optical fiber sensor was proposed based on a side-polished microfiber structure. By controlling the waist diameter of side-polished microfiber, the sensitivity of the sensor can be controlled. The developed sensor is thus functionalized with antibody hCG-β-mAb for hCG detection. A mixed solution of hCG and other biomaterials, such as E.Coli, IgG and S. aureus has been used for specificity test and the detection limit is as high as 0.058 mIU/mL with excellent specificity.

II. Theoretical Background and Simulation

Figure 1 (a) is a schematic of the side-polished microfiber structure. Firstly, a single mode fiber (SMF) was side-polished by an optical fiber polishing system. The side-polished fiber was then placed in an optical fiber tapering system to be stretched to a microfiber with outer diameters varying from 6 to 30 micrometers. From the Scanning Electron Microscope image shown in Figure 1(b), the side-polished surface can be observed clearly.

In Figure 1(a), as the fundamental mode transmits from SMF to the tapered side-polished (TSP) fiber, multiple modes will be excited due to the surrounding RI of the TSP fiber is much smaller than that of the silica. These multiple modes will transmit independently within the TSP fiber and couple to the core of the output SMF, where the interference will take place, resulting in transmission peaks and dips in the output spectrum. When the surrounding RI changes, the eigen modes in the TSP fiber will change, thus altering the phase difference of these modes and causing a wavelength shift in the output spectrum. By monitoring the wavelength variation of the TSP fiber sensor, the surrounding RI will be determined. The very detailed theoretical background analysis of an SMS fiber structure can be found in [8].

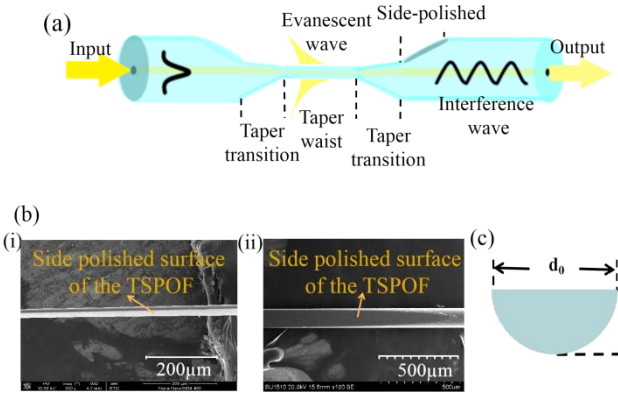

Fig. 1. (a) A schematic diagram of the TSP fiber structure; (b) SEM image of a part of side polished region, (i) side view and (ii) front view of the structure; (c) a schematic diagram of the cross section of the TSP fiber.

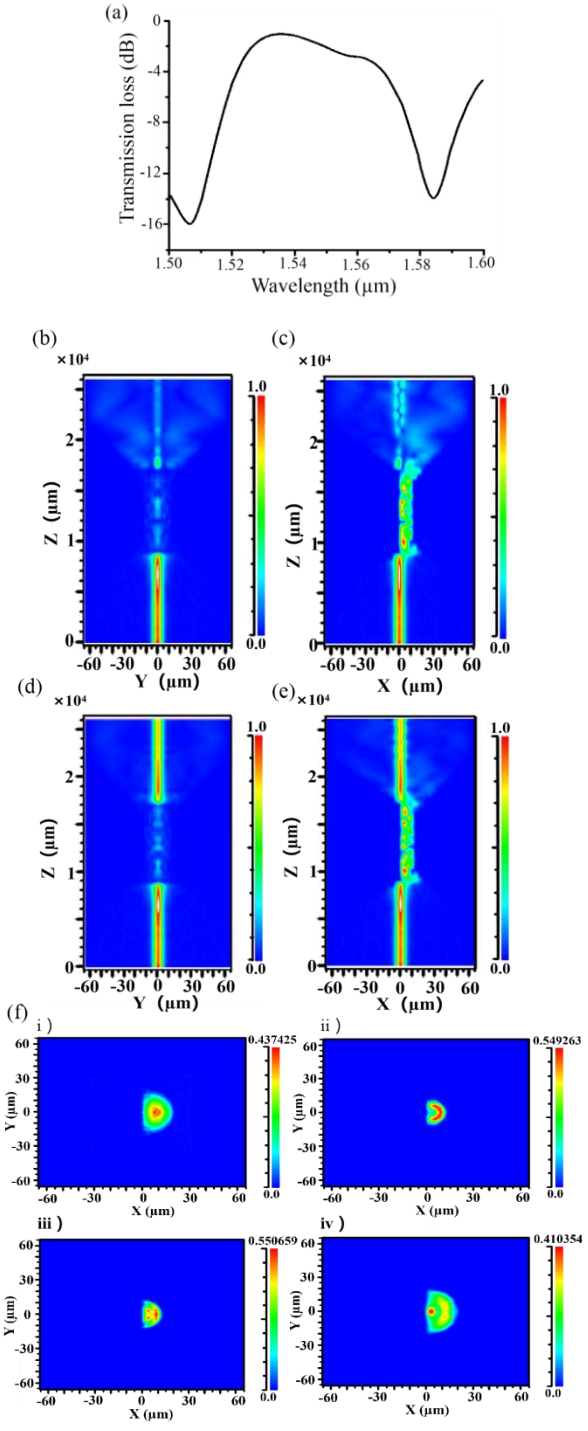

Fig. 2. Simulated results of the TSP fiber sensor, (a) the transmission spectrum of the sensor; optical field distribution at 1506.5 nm (dip) along (b) X-Z and (c) Y-Z direction; optical field distribution at 1535 nm (peak) along (d) X-Z and (e) Y-Z direction; (f) optical field distribution of cross sections at 1535 nm, at i) Z =0.9, ii) Z =1.2, iii) Z =1.4 and iv) Z =1.7 cm

A numerical simulation study of the TSP fiber sensor was executed using the beam propagating method (BPM). The mesh size of the 3D model in the simulation are X, Y (0.5 μm) and Z (2 cm). The model boundary conditions are based on fully matched layer conditions. The core/cladding diameter of the SMF are set to 9/125 μm. The RI of the core/cladding are 1.4428/1.4507, respectively, and the RI of the surrounding material of the TSP fiber is 1.34. During the numerical simulation process, the two taper transition lengths in both ends and the length of the taper waist are 6 mm. The cross-section of the taper waist region is D-shaped as shown in Figure 1(c), the taper waist diameter d_0 and d_1 were set to 24 and 12 μm, respectively. Figure 2(a) shows the spectral response of the TSP fiber sensor, where a strong mode interference can be observed in the wavelength range 1500 nm to 1600 nm. Figures 2(b) and (c) show the power transmission of the TSP fiber sensor along the X-Z and Y-Z direction respectively when the wavelength is 1506.5 nm, where very limited power is transmitted to the output SMF in both directions. Figures 2(d) and (e) show the optical field transmission of the TSP along x-z and y-z direction at peak wavelength 1536 nm, respectively. In addition, obvious D-shape optical field evolutions of cross-section (X-Y direction) for the TSP fiber structure can be demonstrated in Figure 2(f).

III. Experimental Investigation

A. The TSP fiber Structure for RI Measurement

A section of standard Corning SMF-28 (9/125 μm core/cladding diameter) is polished using a self-assembled fiber side polishing system [40]. In the system, the residual diameter of the polished fiber is calibrated by real-time measuring the output optical power of the fiber during the side-polishing process. In our experiments, the polish length is 8 mm, and the polish depth is about 57.69 μm. The side polished SMF is then tapered to smaller diameter at the range between 6 μm to 30 μm.

Firstly, the RI sensitivity of the TSP fiber sensor was studied. Figure 3 shows a schematic setup used in the experiment. The light emitted by a supercontinuum light source (SCLS: SC-5) is injected into the TSP structure and the output signal is connected to an optical spectrum analyzer (OSA, AQ6370D). The RI liquid sample was made by mixing the dimethyl sulfoxide with deionized water with different weight ratio and thus different RI whose value was calibrated by an Abbe refractometer. The TSP fiber sensor was immersed into the prepared RI solution and the wavelength shifts will be recorded. Figure 4 shows the wavelength shifts of the TSP vs. RI with different taper waist diameter. It is clear to see in Figure 4 that the sensitivity of RI increases from 2640.15 to 14219.61 nm/RIU as the taper diameter of the side-polished fiber decreases from 23.7 to 6.3 μm. Figures 5(a), (c) and (e) are the measured spectra of the TSP optical fiber sensor with a taper diameter 6.3 μm in three different RI ranges: 1.33-1.34, 1.37-1.38 and 1.40-1.41, respectively. Figures 5(b), (d) and (f) show the corresponding linear fit of the sensing wavelength shift vs. RI. From these figures, we can find, with the same waist diameter of 6.3, the RI sensitivity increases as the RI increases,

and the highest RI sensitivity is 14219.61 nm/RIU in RI range of 1.4022-1.4062.

Fig. 3. A schematic experimental setup for RI and hCG measurement.

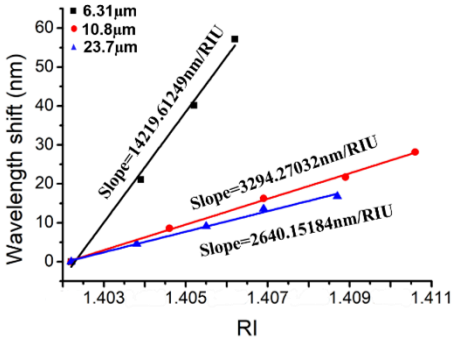

Fig. 4. Calculated sensitivity of different waist diameter in the RI range of 1.4.

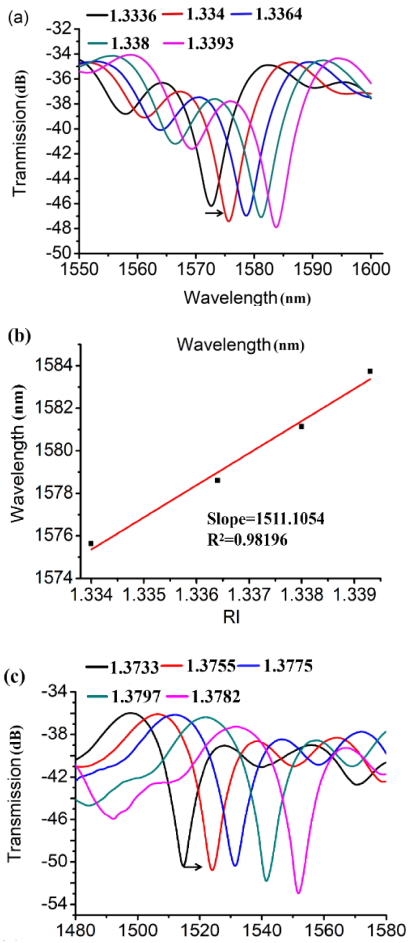

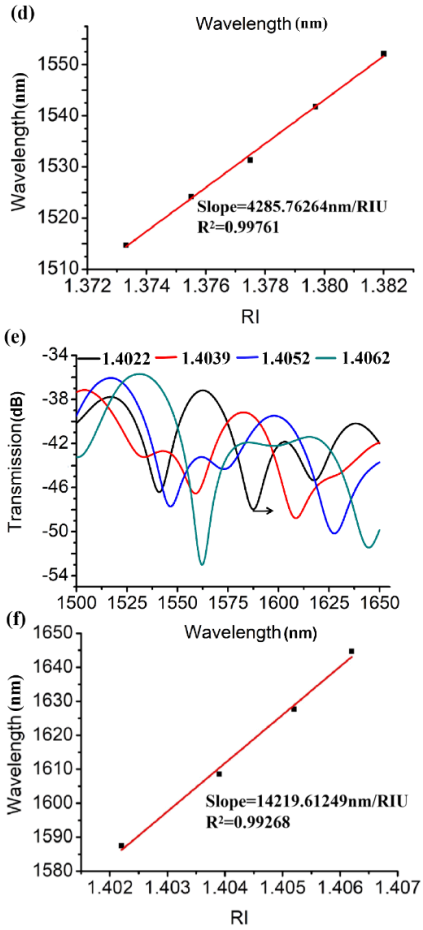

Fig. 5. (a), (c) and (e) are the shift of the wavelength dips; (b), (d) and (f) described the corresponding sensitivity and linear correlation coefficient in the RI range of 1.33-1.34, 1.37-1.38 and 1.40-1.41, respectively.

B. STP optical fiber sensor for hCG detection

In order to realize hCG sensing, the STP fiber sensor was functionalized with hCG-β-mAb, an antibody that will specifically bind to hCG. If the hCG is bind to the antibody hCG-β-mAb immobilized on the STP fiber surface, the physical property (effective surrounding RI) of the TSP fiber sensor will change, resulting in a resonant wavelength shift. Once the wavelength shift vs. hCG concentration is calibrated, the functionalized TSP sensor can be used for hCG detection. Based on the above RI sensitivity investigation, the TSP fiber sensor with the waist diameter ~6 μm was selected for hCG detection since it has highest RI sensitivity. Prior to functionalization of the fiber optic sensor, the TSP fiber sensor was firstly immersed into a standard solution of potassium hydroxide -ethanol for one hour to clean the fiber, then washed by deionized (DI) water for three times until the washed water was in neutral (pH=7), and then dried at ambient environment. After cleaning the fiber, the fiber will be functionalized with the following steps as illustrated in Figure 6:

i: Formation of carboxyl group: immerse the fiber sensor into 5% silane reagent (3-(Triethoxysilyl) propylsuccinic anhydride) (configured by 95% silane reagents and 99.99%

ethanol solution) for 4 hours. This process will create carboxyl group on the surface of fiber sensor.

ii: Activate succinimide ester: use ethanol and Phosphate buffer (PB, pH=6.0, without sodium chloride) to wash the sensor and remove the remained silane reagent solution, then treat with the mixture solutions contained 0.8 mg/mL EDC (1-(3-Dimethylaminopropyl)-3-ethylcarbodiimide hydrochloride) and 1.2 mg/mL N-Hydroxysulfosuccinimide sodium salt (NHSS) for one hour. This step aims to obtain an activated succinimide ester, which was formed by EDC reacted with NHSS, on the surface of the fiber.

iii: Antibody immobilization: immerse the fiber sensor into Phosphate buffer saline (PBS) to wash the residual solution. The fiber sensor was then immersed in a 50 μg/mL solution of anti hCG-β-mAb for 4 hours.

iv: Nonspecific bind block: the antibody immobilized fiber sensor was washed with PBS and then treated with 1% Bovine serum albumin (BSA) solution for 2 hours at room temperature. This process is to block the fiber surface without immobilized antibody, thereby suppress nonspecific bind.

v: Before use the functionalized fiber sensor for hCG solution, use PBS to wash the sensor.

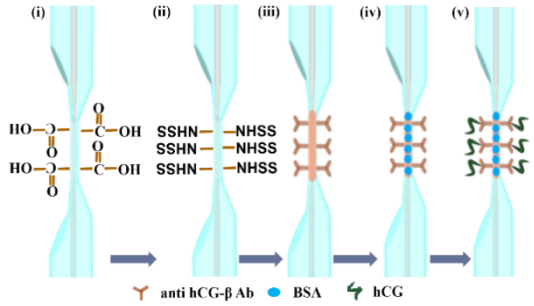

Fig. 6. Schematic diagram of immobilizing anti hCG-β-mAb on the fiber sensor surface: (i) formation of carboxyl group; (ii) activate succinimide ester; (iii) antibody immobilization; (iv) nonspecific bind block; (v) detection of hCG.

After functionalizing the TSP optical fiber, put it into a microchannel to detect a different concentration of hCG solution. During the hCG detection procession, four concentrations of hCG (0.1, 1, 10, 100 mIU/mL) were prepared. Before detecting every hCG concentration, the stability of the sensor was tested in PBS solution, and the result show this sensor has good stability as described in Figure 7(a). It shows that the wavelength variation in 30 minutes is ±0.15 nm, demonstrating good stability of the developed TSP biosensor. Figure 7(b) shows the spectra of the functional TSP sensor (with 50 μg/mL of anti hCG-β-mAb) immersed in a 0.1 mIU/mL hCG solution for a period of time. As show in Figure 7(b), the wavelength dip in the output spectrum shifts towards a shorter wavelength over time, which took place in the initial 6 minutes and after 20 minutes, there is almost no wavelength shift. Figure 7(c) shows an example of summarized the measured wavelength shift vs. time using the TSP fiber sensor to detect above four different hCG solutions. It is noted that during the hCG detection, the hCG samples start from the low concentration of 0.1 mIU/mL to high concentration of 100 mIU/mL, and before each measurement of different hCG concentration, the sensor will be washed by PBS to remove the non-specific bounded hCG.

Sensor reproducibility was studied by manufacturing four fiber sensors with same side-polish, tapering parameters and surface modification conditions (hCG-β-mAb). Figure 7(d) illustrates the measured result, where reasonable good error bar for hCG concentration varies from 10^{-1} to 10^{2} mIU/mL, indicating good reproducibility of the proposed sensor. Figure 7(e) plots the average wavelength shift at different concentration of hCG and its fitted curve. As shown in Figure 7(d), when the hCG concentration is 0.1 mIU/mL, the average wavelength shift of the TSP sensor is 0.82 nm. According to the fitted curve, the average wavelength shift y can be express as a function of hCG concentration x:

$$y = 2.23 + 1.44log_{10}^{x} \qquad (1)$$

Because the peak-to-peak wavelength average change in PBS within 30 min is ±0.15 nm, 3 times peak-to-peak change (3×0.15=0.45 nm) is defined as the limit of measurement. In this case, according to Eq. (1), the LoD of the hCG is calculated as 0.058 mIU/mL. It is noted that in each hCG experiment, several fiber sensor samples will be functionalized, and the functionalized fiber sensor will be stored in fridge at 4 ℃. Our experimental results show that after four or five days, there is no significant performance degradation of the sensor for hCG detection. Table 1 shows a compare between the performance of our develop sensor and previous published techniques.

Table 1. Comparative performance of the developed hCG sensing platforms with the previously reported techniques

Sensor type	Concentration range	Sensitivity	Limit of detection	Ref.
SPR	4.16-250 nM	-38.34 m°/nM	0.065 nM	[41]
Aolorimetric assay	1 mIU/mL-0.21 IU/mL	-	0.4 mIU/mL	[42]
Microtoroid optical resonators	100 aM-10 nM	-	120 aM	[43]
Electrochemical	0-1000 pg/mL	1 pg/mL	100 pg/mL	[44]
Tapered Hollow core optical fiber	5-500 mIU/mL	0.1 nm/(mIU/mL)	0.6 mIU/mL	[5]
Tapered no-core optical fiber	0.05-500 mIU/mL	98 nm/(mIU/mL)	0.0001 mIU/mL	[38]
TSP optical fiber	0.1-100 mIU/mL	1.44 nm/(mIU/mL)	0.058 mIU/mL	This work

To study the specificity of the tapered side-polished biosensor, three different biomaterials, pig-IgG (1 μg/mL), *Staphylococcus aureus* (*S. aureus*) (6×10^5 CFU/mL) and *Escherichia coli* (*E. coli*) (2.5×10^5 CFU/mL) were used to detect the wavelength shift by immersing the developed biosensor into these biomaterials in sequence. The measured wavelength shift vs. time in the three biomaterials is shown in Figure 8(a), which have similar wavelength shift to that of PBS, indicating that the functionalized sensor has no specific bind with these biomaterials. To simulate real world situation, we use a mixture solution of pig-IgG (1 μg/mL), S. aureus (6×10^5 CFU/mL), E. coli (2.5×10^5 CFU/mL) and hCG (1 mIU/mL) to investigate the specificity of the sensor and the measured wavelength shift is shown in Figure 8(b). The results show that the developed fiber sensor has excellent specific detection of hCG. It can also be seen in Figure 8(b) that the wavelength shift in mixed solution is slightly smaller than that in pure hCG solution. This is possibly due to the fact that other biomaterials have impact to decrease the bind activity and capability of the functionalized antibody hCG-β-mAb.

The influence of temperature on the performance of the TSPOF was studied and the result is shown in Figure 9(b). It can be seen that as temperature varies from 20 to 40 ℃, the wavelength shift is 0.27 nm. In our experiment, the test is conducted in room temperature, and the detection is the "dynamic" measurement of wavelength shift between the wavelength before and after adding the analyte liquid into the container of the biosensor. Since the measuring process is not long and the surrounding temperature variations is normally less than 2 ℃ within 30 minutes, the temperature induced wavelength shift in the experiment is less than 0.02 nm, which is much smaller than the wavelength shift in the stability test (±0.15 nm), indicating that the influence of temperature on the sensor performance is very limited.

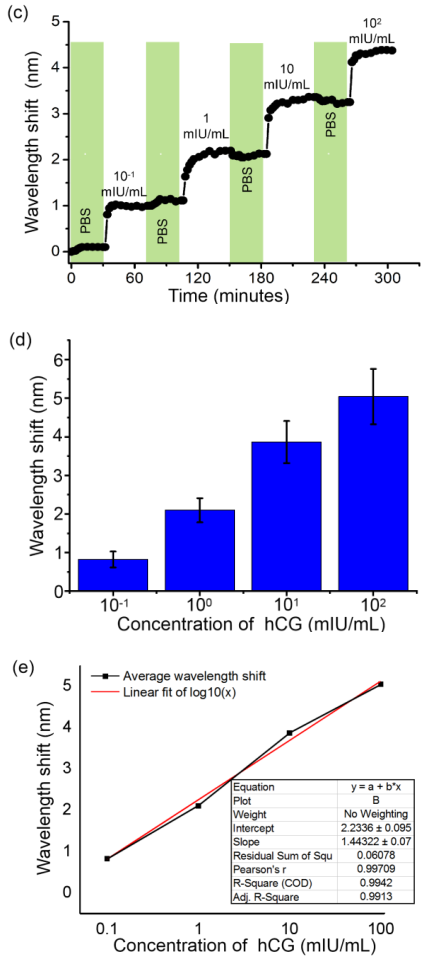

Fig. 7. (a) The measured wavelength shift of the sensor in the PBS solution before detecting the four different concentrations of hCG solutions; (b) the spectral response when the sensor is immersed into hCG (0.1 mIU/mL) solution; (c) summarized the wavelength shift with the time increasing in different concentration of hCG; (d) the wavelength shift error bar in different hCG concentration; (e) average wavelength shift vs. hCG concentration and fitted curve.

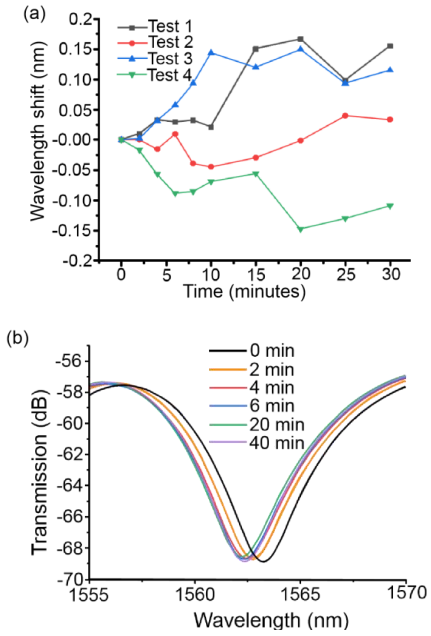

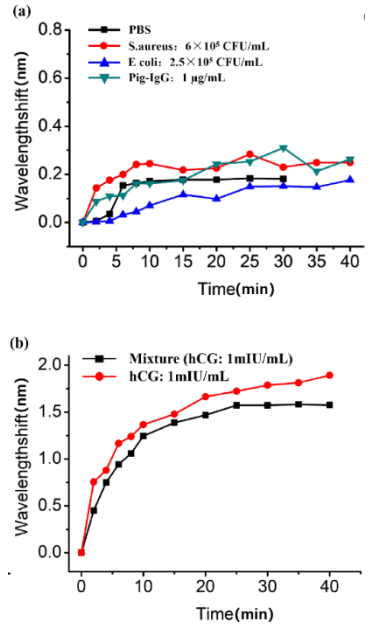

Fig. 8. The wavelength shift during immersing the sensor into the (a) E. coli, S. aureus, PBS and pig-IgG solution; and (b) pure hCG and mixture solution.

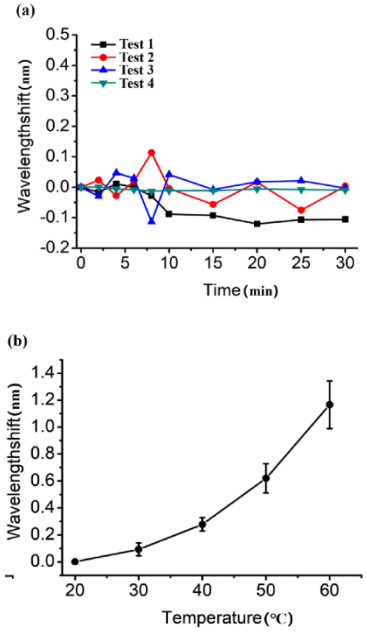

Fig. 9. (a) Stability test of the biosensor in room temperature; (b) wavelength shift error bar vs. temperature.

IV. Conclusions

In conclusion, a novel optical fiber hCG sensor based on TSP fiber structure is proposed and investigated. The RI sensing experiment shows that the TSP fiber sensor with a taper waist diameter of 6.3 and residual depth of ~67 μm has RI sensitivity 1511.10 and 14219.61 nm/RIU in RI range 1.334-1.349 and 1.402-1.407 respectively. The developed TSP optical fiber is functionalized with 50 μg/ml hCG-β-mAb to detect hCG concentration. The result shows a low LoD of 0.058 mIU/mL. Specifically, we immerse the fiber structure into the pure hCG solution and mixture solution of pig-IgG, S. aureus, E. coli and hCG (1 mIU/mL) to investigate the specificity of the sensor. The temperature influence on the performance of the hCG sensor was studied. As the temperature changes from 20 to 40 °C, the wavelength shift is 0.27 nm, which is smaller than that of wavelength fluctuation (0.45 nm) in PBS, indicating that the temperature has very limited impact on the performance of the sensor. The proposed biosensor has good repeatability and specificity, which has excellent potential in medical diagnosis, environmental monitoring and food safety application.

References

[1] M. F. S. Ferreira, E. C. Camus, D. J. Ottaway, J. M. L. Higuera, X. Feng, W. Jin, Y. Jeong, N. Picqué, L. M. Tong, B. M. Reinhard, P. M. Pellegrino, A. Mendez, M. Diem, F. Vollmer and Q. M. Quan, "Roadmap on optical sensors," Journal of Optics, vol. 19, no. 8, 2017. 083001.

[2] M. Ahmad and L. L. Hench, "Effect of taper geometries and launch angle on evanescent wave penetration depth in optical fibers," Biosensors and Bioelectronics, vol. 20, no. 7, pp. 1312-1319, 2005.

[3] Q. Wu, Y. Semenova, P. F. Wang and G. Farrell, "High sensitivity SMS fiber structure based refractometer-analysis and experiment," Optics Express, vol. no. 19, pp. 7937-7944, 2011.

[4] H. W. Qiu, S. S. Gao, P. X. Chen, Z. Li, X. Y. Liu, C. Zhang, Y.Y. Xu, S. Z. Jiang, C. Yang, Y.Y. Huo and W. W. Yue, "Evanescent wave absorption sensor based on tapered multimode fiber coated with monolayer graphene film," Optics. Communications, vol. 366, pp. 275-281, 2016.

[5] L. Chen, B. Liu, J. Liu, S. P. Wang, T. Wu, J. H. Yuan, X. Zhou, K. P. Long, L. Y. Shao, Y. Q. Fu, X. D. He and Q. Wu, "Novel Microfiber Sensor and Its Biosensing Application for Detection of hCG Based on a Singlemode-Tapered Hollow Core-Singlemode fiber Structure," IEEE Sensors Journal, vol. 99, no. 16, pp. 1-1, 2020.

[6] S. Kaushik, U. Tiwari, S. Prashar, B. Das and R. K. Sinha, "Label-free detection of escherichia coli bacteria by cascaded chirped long period gratings immunosensor, " Review of Scientific Instruments, Nol. 90, No. 2, Num. 025003, 2019.

[7] S. Kaushik, A. Pandey, U. K. Tiwari and R. K. Sinha, "A label-free fiber optic biosensor fo rsalmonella typhimurium detection, " Optical Fiber Technology, Vol. 46, pp. 95-103, 2018.

[8] Q. Wu, Y. W. Qu, J. Liu, J. H. Yuan, S. P. Wang, T. Wu, X. D. He, B. Liu, D. J. Liu, Y. Q. Ma, Y. Semenova, X. J. Xin, P. Wang and G. Farrell, "Singlemode-Multimode-Singlemode fiber Structures for Sensing Applications - A Review," IEEE Sensors Journal, vol. 21, no. 11, pp. 12734-12751, 2021.

[9] J. Y. Lou, Y. P. Wang and L. M. Tong, "Microfiber Optical Sensors: A Review," Sensors, vol. 14, no. 4, pp. 5823-5844, 2014.

[10] H. E. Joe, H. Yun, S. H. Jo, M. B. G. Jun and B. K. Min, "A review on optical fiber sensors for environmental monitoring," International Journal of Precision Engineering and Manufacturing-Green Technology, vol. 5, no. 1, pp. 173-191, 2018.

[11] L. M. Tong, R. R. Gattass. J. B. Ashcom, S. L. He, J. Y. Lou, M. Y. Shen, I. Maxwell and E. Mazur, "Subwavelength-Diameter Silica Wires for Low-Loss Optical Wave Guiding," Nature, vol. 426, no. 6968, pp. 816-819, 2003.

[12] G. Brambilla, F. Xu, P. Horak, Y. Jung, F. Koizumi, N. P. Sessions, E. Koukharenko, X. Feng, G. S. Murugan, J. S. Wilkinson and D. J. Richardson, "Optical fiber nanowires and microwires: fabrication and applications," Advances in Optics & Photonics, vol. 1, no. 1, pp. 107-161, 2009.

[13] L. M. Tong, F. Zi, X. Guo and J. Y. Lou, "Optical microfibers and nanofibers: A tutorial," Optics Communication, 2vol. 85, no. 23, pp. 4641-4647, 2012.

[14] W. Luo, Y. Chen and F. Xu, "Recent Progress in Microfiber-Optic Sensors," Photonic Sensors, vol. 11, no. 1, pp. 45-68, 2021.

[15] L. Zhang, Y. Tang and L. M. Tong, "Micro-/Nanofiber Optics: Merging Photonics and Material Science on Nanoscale for Advanced Sensing Technology," iScience, vol. 23, no. 1, num. 100810, 2020.

[16] B. S. Kawasaki, K. O. Hill and R G Lamont, "Biconical-taper single-mode fiber coupler," Optics Letters, vol. 6 no. 7, PP. 327-328, 1981.

[17] L. L. Xu, Y. Li and B. J. Li, "Nonadiabatic fiber taper-based Mach-Zehnder interferometer for refractive index sensing," Applied Physics Letters, vol. 101, no. 15, pp. 2467, 2012.

[18] L. Chen, Y. Leng, B. Liu, J. Liu, S. Wan, T. Wu, J. Yuan, L. Shao, G. Gu, Y. Q. Fu, H. Xu, Y. Xiong, X. D. He, Q. Wu, "Ultrahigh-sensitivity label-free optical fiber biosensor based on a tapered singlemode-no core-singlemode coupler for Staphylococcus aureus detection", Sensors and Actuators B-Chemical, vol. 320, pp. 128283, 2020.

[19] I. M. White, H. Oveys and X. D. Fan, "Liquid-core optical ring-resonator sensors," Optics Letters, vol. 31, no. 9, pp. 1319-1321, 2006.

[20] K. Markowski, K. Jedrzejewski, M. Marzecki, and T. Osuch, "Linearly chirped tapered fiber - Bragg - grating-based Fabry – Perot cavity and its application in simultaneous strain and temperature measurement," Optics Letters, vol. 42, no. 7, pp. 1464-1467, 2017.

[21] T. Osuch, K. Markowski, K. Jedrzejewski, "fiber-Optic Strain Sensors Based on Linearly Chirped Tapered fiber Bragg Gratings With Tailored Intrinsic Chirp," IEEE Sensors Journal, vol. 16, no. 20, pp. 7508-7514, 2016.

[22] B. C. Yao, C. B. Yu, Y. Wu, S. W. Huang, H. Wu, Y. Gong, Y. F. Chen, Y. R. Li, C. W. Wong, X. D. Fan and Y. J. Rao, "Graphene-Enhanced Brillouin Optomechanical Microresonator for Ultrasensitive Gas Detection," Nano Letters,vol. 17, no. 8, pp. 4996-5002, 2017.

[23] M. A. Gouveia, P. E. S. Pellegrini, J. S. Santos, I. M. Raimundo and C. M. B. Cordeiro, "Analysis of immersed silica optical microfiber knot resonator and its application as a moisture sensor," Applied Optics, vol. 53, no. 31, pp. 7454-61, 2014.

[24] Y. Ying, G. Y. Si, F. J. Luan, K. Xu, Y. W. Qi and H. N. Li, "Recent research progress of optical fiber sensors based on D-shaped structure," Optics and Laser Technology, vol. 90, pp. 149-157, 2017.

[25] N. N. Luan, R. Wang, W. H. Lv and J. Q. Yao, "Surface plasmon resonance sensor based on D-shaped microstructured optical fiber with hollow core," Optics Express, vol. 23, no. 7, pp. 8576-8582, 2015.
[26] R. K. Gangwar and V. K. Singh, "Highly Sensitive Surface Plasmon Resonance Based D-Shaped Photonic Crystal fiber Refractive Index Sensor," Plasmonics, vol. 12, no. 5, pp. 1367-1372, 2017.
[27] N. A. A. Kadir, M. H. A. Wahid, M. Q. Lokman, N. Irawati, A. Hamzah and S. W. Harun, "Side-Polished Optical fiber Structure for Sodium Nitrate Sensor," IEEE Sensors Journal, vol. 20, no. 11, pp. 5929-5934, 2020.
[28] N. A. A. Kadir, N. Irawati, A. A. A. Jafry, N. M. Razali, A. Hamzah and S. W. Harun, "Sodium Nitrate Sensor Based on D-shaped fiber Structure," Measurement, vol. 163, 2020.
[29] S. F. Wang, M. H. Chiu and R.S. Chang, "Numerical simulation of a D-type optical fiber sensor based on the Kretchmann's configuration and heterodyne interferometry," Sensors and Actuators B-Chemical, vol. 114, no. 1, pp. 120-126, 2006.
[30] X. Chen, L. Xia and C. Li, "Surface plasmon resonance sensor based on a novel D-shaped Photonic Crystal fiber for low refractive index detection," IEEE Photonics Journal, vol. 10, no. 1, pp. 1-9, 2018.
[31] H. M. Huang, Y. Yu, L. J. Zhou, Y. Y. Tao, J. B. Yang and Z. R. Zhang, "Whispering gallery modes in a microsphere attached to a side-polished fiber and their application for Magnetic field sensing", Optics Communications, vol. 478, 2020.
[32] H.-J. Kim, O. J. Kown, S. B. Lee and Y. G. Han, "Measurement of temperature and refractive index based on surface long-period gratings deposited onto a D-shaped photonic crystal fiber," Applied Physics B-laser and Optics, vol. 102, no. 1, pp. 81-85, 2011.
[33] J. N. Dash and R. Jha, "On the Performance of Graphene-Based D-Shaped Photonic Crystal Fiber Biosensor Using Surface Plasmon Resonance," Plasmonics, vol. 10, no. 5, pp. 1123-1131, 2015.
[34] S. Damiati, C. Haslam, S. Sopstad, M. Peacock, T. Whitley, P. Davey and S. A. Awan, "Sensitivity Comparison of Macro- and Micro-Electrochemical Biosensors for Human Chorionic Gonadotropin (hCG) Biomarker Detection," IEEE Access, vol. 7, pp. 94048-94058, 2019.
[35] M. Tsampalas, V. Gridelet, S. Berndt, J. M. Foidart, V. Geenen and S.P.Dhauterive, "Human chorionic gonadotropin: A hormone with immunological and angiogenic properties," Journal of Reproductive Immunology, vol. 85, pp. 93-98, 2010.
[36] C.Ticconi, A. Zicari, A. Belmonte, M. Realacci, C. V. Rao and E. P iccione, "Pregnancy-Promoting Actions of HCG in Human Myometrium and Fetal Membranes," Placenta 28. supp-S (2007) S137-S143.
[37] S. Hoshi, K. I. Suzuki, S. Ishidoya, C.Ohyama, M. Stato, T.Namima, S. Saito and S. Orikasa, "Significance of simultaneous determination of serum human chorionic gonadotropin (hCG) and hCG-β in testicular tumor patients," International Journal of Urology, vol. 7, no. 6, pp. 218-223, 2000.
[38] R. Kumar, Y. K. Leng, B. Liu, J. Zhou, L. Y. Shao, J. H. Yuan, X. Y. Fan, S. P. Wan, T. Wu, J. Liu, R. Binns, Y. Q. Fu, W. P. Ng, G. Farrell, Y. Semenova, H. Y. Xu, Y. H. Xiong, X. D. He and Q. Wu, "Ultrasensitive biosensor based on magnetic microspheres enhanced microfiber interferometer," Biosensors & Bioelectronics, vol. 145, 2019.
[39] Elçin Ezgi Ahi, Hilal Torul, Adem Zengin, Ferah Sucularlı, Ender Yıldırım, Yeşim Selbes, Zekiye Suludere and Uğur Tamer, "A capillary driven microfluidic chip for SERS based hCG detection," Biosensors & Bioelectronics, vol. 195, Jan. 2022.
[40] P. Zhang, B. Liu, J. Liu, C. F. Xie, S. P. Wang, X. D. He, X. P. Zhang and Q. Wu, "Investigation of a Side-Polished fiber MZI and Its Sensing Performance," IEEE Sensors Journal, vol. 20, no. 11, pp. 5909-5914, Jun 2020
[41] C. Nan Fu, K. Chia Tzu, L. Ting Li, C. Chia Chen and C. Chen Yu, "Ultra-high sensitivity of the non-immunological affinity of graphene oxide-peptide-based surface plasmon resonance biosensors to detect human chorionic gonadotropin," Biosensors & Bioelectronics, 2017, DOI: http://dx.doi.org/10.1016/j.bios.2017.03.008.
[42] X. Ning, C. Zhihua, L. Yadong, R. Huizhu and L. Lin, "Peptide aptamer-based biosensore for the detection of human chorionic gonadotropin by converting silver nanoparticles-based colorimetric assay into sensitive electrochemical analysis," Sensors and Acruators B: Chemical, Vol. 243, pp. 784-791, 2017.
[43] C. Ozgur, K. E. Roberts, E. O. Ozgur, A. N. Gin and J. Su, "Ultra-sensitive detection of human chorionic gonadotropin using frequency locked microtoroid optical resonators," Analytical Chemistry, Vol. 91, No. 18, 2019.
[44] S. Damiati, C. Haslam, S. Sopstad, M. Peacock and S. A. Awan, "Sensitivity comparison of macro- and micro-electrochemical biosensors for human chorionic gonadotropin (hcg) biomarker detection," IEEE Access, Vol. 7, pp. 94048-94058, 2019.